# Density Functional Theory Study of the Binding Capability of Tris(pyrazol-1-yl)methane toward Cu(I) and Ag(I) Cations

**Maurizio Casarin,*,†,‡,§ Daniel Forrer,†,§ Federica Garau,† Luciano Pandolfo,†,§ Claudio Pettinari,|| and Andrea Vittadini‡,§**

*Dipartimento di Scienze Chimiche, Università degli Studi di Padova, Padova 35131, Italy, Dipartimento di Scienze Chimiche, Università degli Studi di Camerino, Camerino (MC) 62032, Italy, Istituto di Scienze Molecolari del CNR, Padova 35131, Italy, and Consorzio Interuniversitario di Scienza e Tecnologia dei Materiali, Firenze 50121, Italy*

*Received: March 4, 2008; Revised Manuscript Received: April 28, 2008*

Density functional theory (DFT) has been used to look into the electronic structure of $[M(tpm)]^+$ molecular ion conformers (M = Cu, Ag; tpm = tris(pyrazol-1-yl)methane) and to study the energetics of their interconversion. Theoretical data pertaining to the free tpm state the intrinsic instability of its $\kappa^3$-like conformation, thus indicating that, even though frequently observed, the $\kappa^3$-tripodal coordinative mode is unlikely to be directly achieved through the interaction of M(I) with the $\kappa^3$-like tpm conformer. It is also found that the energy barrier for the $\kappa^2$-$[M(tpm)]^+ \rightarrow \kappa^3$-$[M(tpm)]^+$ conversion is negligible. As far as the bonding scheme is concerned, the tpm $\rightarrow$ M(I) donation, both $\sigma$ and $\pi$ in character, is the main source of the M(I)−tpm bonding, whereas back-donation from completely occupied M(I) d orbitals into tpm-based $\pi^*$ levels plays a negligible role.

## 1. Introduction

Tris(pyrazol-1-yl)borate (hereafter, tp) and tris(pyrazol-1-yl) methane (hereafter, tpm) are considered among the most useful ligands in modern coordination chemistry.[1] Substituted and unsubstituted tp and tpm supply in fact a significant steric shielding of the metal center serving, at the same time, as reliable spectator ligands. These peculiarities make them useful for the synthesis of complexes with virtually all metals in the periodic table, having thus applications in diverse and important fields ranging from catalysis to biomedicine, from metal extraction to biomimetic inorganic chemistry.[1f,g,h,i] In general, tp and tpm behave as tripodal $\kappa^3$-ligands through the lone pairs of the nitrogen heteroatoms [N(•)] of the three pyrazolyl fragments (see Figure 1d).[2] In this regard, these ligands are often labeled as scorpionates, a consequence of an oneiric description of their bonding capabilities where, like the pincers of a scorpion, the N(•) of two pyrazolyl moieties attached to B (tp) or C (tpm) bind a metal, and the third pyrazolyl attached to the central atom rotates forward like the scorpion's tail to "sting" the metal. Although such a picture is certainly attractive, crystallographic data pertaining to the free tp[3a] and tpm,[4] i.e., the simplest members of the scorpionate family, suggest alternative bonding mechanisms. In fact, both tp and tpm solid state structures are characterized by a single pyrazolyl group with N(•) in trans with respect to the H atom of the B−H (tp)/C−H (tpm) fragments (see Figure 1b).[5]

Theoretical work so far devoted to the study of tp and tpm ligands with metal ions is very limited. De Bari and Zimmer[7] carried out a study of the conformational flexibility of tp and tpm behaving as $\kappa^3$-tripodal ligands showing, through the use of molecular mechanics and database analysis, that "tripodal scorpionate ligands can accommodate a variety of metal sizes by opening up the ligand".

In this paper we present and discuss the results of a series of first-principle numerical experiments devoted to the study of the electronic structure of $\kappa^1$-monodentate, $\kappa^2$-chelating, and $\kappa^3$-tripodal $[M(tpm)]^+$ molecular ions (M = Cu, Ag) as well as to the energetics of their interconversion.[8] The first section of the contribution is dedicated to the theoretical analysis of the free pyrazole molecule (hereafter, Hpz)[9] and its hypothetical $[M(Hpz)]^+$ $\sigma$ and $\pi$ complexes with the aim of gaining quantitative information about the nature and the strength of the M(I)−Hpz interaction. The second part deals with the conformation flexibility of the free tpm ligand, leaving aside any problem concerning optical isomerism, and the third one is focused on binding energies and electronic properties of the $[M(tpm)]^+$ molecular ions.

## 2. Computational Details

All the numerical experiments have been carried out by using the Amsterdam Density Functional (ADF) package[12] and adopting the scalar relativistic zeroth-order regular approximation (ZORA).[13] Optimized geometries for ground and transition states (GS and TS, respectively) were obtained by employing generalized gradient (GGA) corrections self-consistently included through the Becke−Perdew formula,[14] and without imposing any symmetry. All TS's have been estimated through the following procedure: (i) a linear transit (LT) calculation has been run by varying a dihedral angle[15] (vide infra); (ii) from the TS guess provided by step (i), a stationary point on the energy surface has been searched; (iii) the adequacy of the TS estimate has been then checked by computing vibrational frequencies at the corresponding geometry and verifying that one of them is imaginary; (iv) the Hessian computed in the third step is employed for the final TS optimization.

TZP ZORA basis sets were adopted for all the atoms;[16] inner cores of Cu (1s2s2p3s3p), Ag (1s2s2p3s3p3d), C (1s), and N

† Università degli Studi di Padova.
|| Università degli Studi di Camerino.
‡ Istituto di Scienze Molecolari del CNR.
§ Consorzio Interuniversitario di Scienza e Tecnologia dei Materiali.

10.1021/jp801902c CCC: $40.75 
Published on Web 07/01/2008

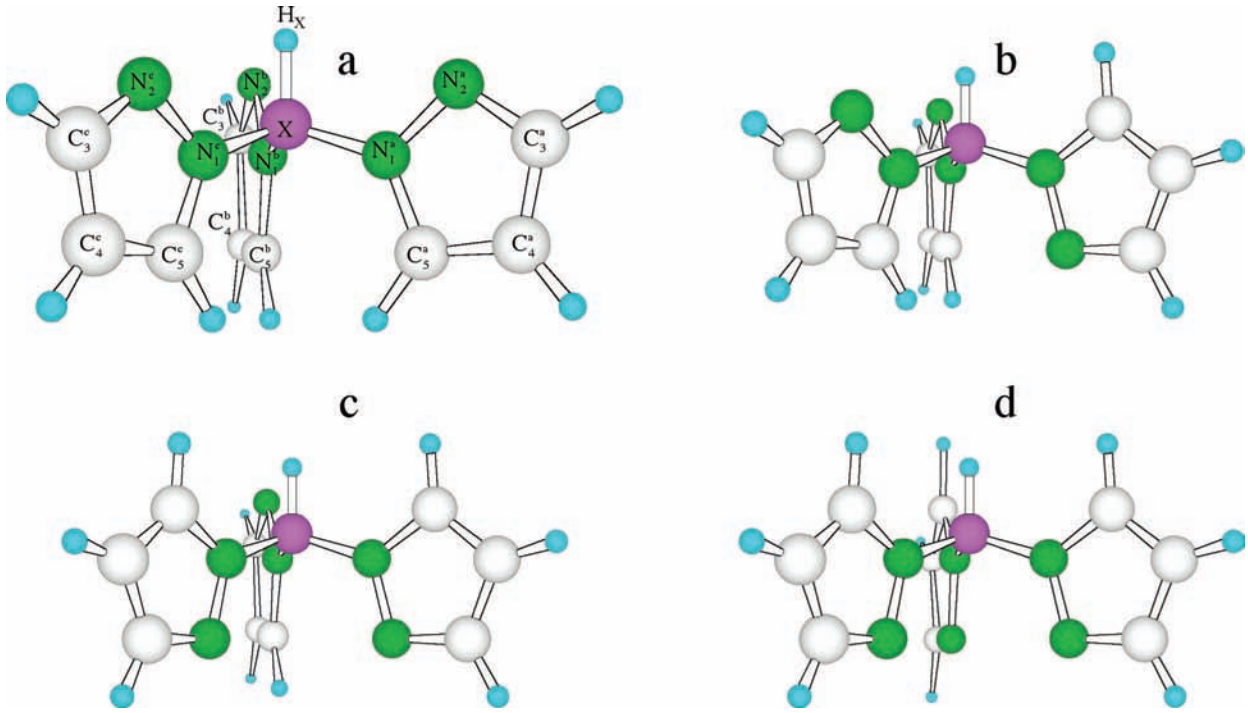


**Figure 1.** Schematic representation of possible relative arrangements of pyrazolyl fragments in tp (X = B) and tpm (X = C).

(1s) atoms were kept frozen throughout the calculations. Binding energies (BEs) were analyzed in terms of fragment molecular orbitals (FMO's) by applying the Ziegler's extended transition state method (ETS).[17] According to the ETS scheme,

$$\mathrm{BE} = \Delta E_{\mathrm{es}} + \Delta E_{\mathrm{Pauli}} + \Delta E_{\mathrm{int}} + \Delta E_{\mathrm{prep}} \qquad (1)$$

where $\Delta E_{\mathrm{es}}$ is the pure electrostatic interaction, $\Delta E_{\mathrm{Pauli}}$ is the destabilizing two-orbital-four-electron interaction between the occupied orbitals of the interacting fragments (($\Delta E_{\mathrm{es}} + \Delta E_{\mathrm{Pauli}}$) corresponds to the so called steric interaction ($\Delta E_{\mathrm{st}}$) contribution), $\Delta E_{\mathrm{int}}$ derives from the stabilizing interaction between occupied and empty orbitals of the interacting fragments, and $\Delta E_{\mathrm{prep}}$ provides information about the energy required to relax the structure of the free fragments to the geometry they assume in the final system. BE's were further corrected by taking into account the basis set superposition error (BSSE) which was estimated by making use of reference energies calculated with "ghost" fragments.[18]

Rather than displaying discrete eigenvalues along an energy axis, we preferred to plot the density of states (hereafter, DOS) as a function of energy by using a 0.25 eV Lorentzian broadening factor. These plots, based on Mulliken's prescription for partitioning the overlap density,[19] have the advantage of providing insights into the atomic composition of MO's over a broad range of energy. Finally, information about the localization and the bonding/antibonding character of selected MO's was obtained by using crystal orbital overlap populations (COOP's)[20] computed by weighting one-electron energy levels by their basis orbital percentage.

## 3. Results and Discussion

As above mentioned, tpm is a potentially tripodal, neutral ligand characterized by the presence of three pyrazolyl moieties bonded to a central methine carbon atom (see Figure 1). Now, Hpz is planar, fully conjugated, and isoelectronic with the cyclopentadienyl anion, but the higher electronegativity of nitrogen (3.04)[21] compared to that of carbon (2.55)[21] determines a higher electronic charge density on N atoms both in the molecular plane and out of it. In consequence of that, each tpm pyrazolyl group may be involved in two competitive metal−ligand bonding mechanisms: a $\sigma$-binding implying the N(•) lone pair (hereafter, $n_{\mathrm{N}}$) and a $\pi$-binding involving the $\pi$ electron density of the aromatic ring. An intimate comprehension of the tpm coordination capabilities necessarily passes through a deep understanding of the $\sigma/\pi$ $[\mathrm{M(Hpz)}]^+$ bonding scheme.

**3.1. Hpz and $\sigma/\pi$ $[\mathrm{M(Hpz)}]^+$ Complexes.** Optimized coordinates of Hpz are reported in Table S1, and selected geometrical parameters and Mulliken[19] and Hirshfeld[22] gross atomic charges are collected in Tables 1 and 2, respectively. The agreement with data obtained by accurate ab initio calculations (CBS-APNO QCISD/6-311G(d,p))[23] is remarkable; moreover, theoretical estimates of the Hpz dipole moment ($\mu$), lowest ionization energies (IEs)[24] and VUV-absorption bands agree very well with experiment.[27]

The Hpz valence manifold includes five $\pi$-like and the $n_{\mathrm{N}}$ MO's. Among them, the $\pi_1$, $\pi_2$, and $\pi_3$ ones (the 8a, 12a, and 13a levels, respectively) and $n_{\mathrm{N}}$ (the 11a MO) are occupied, whereas $\pi_4$ and $\pi_5$ (the 14a and 16a MO's, respectively) are empty; moreover, $\pi_3$ and $\pi_4$ correspond to the Hpz HOMO and LUMO, respectively. 3D-contour plots of the whole Hpz valence manifold are displayed in Figure 2.

The contemporary presence of the aromatic $\pi$ system and of the $n_{\mathrm{N}}$ allows two competitive bonding mechanisms in $[\mathrm{M(Hpz)}]^+$. With reference to the Hpz → M(I) donation, a simple electron count coupled to symmetry arguments and overlap considerations indicate that (i) $n_{\mathrm{N}}$ will limit its involvement to the M(I)−Hpz $\sigma$ bonding; (ii) the Hpz $\pi$ system may contribute to both $\sigma$ and $\pi$ interactions; (iii) M(I) will participate with its s and p virtual atomic orbitals (AO's). As far as the M(I) → Hpz back-donation is concerned, the charge transfer is possible between the fulfilled M(I) d AO's and the Hpz-based $\pi_4$ and $\pi_5$ virtual MO's.

A schematic representation of the optimized structure of $\sigma/\pi$ $[\mathrm{M(Hpz)}]^+$ complexes is displayed in Figure 3 (corresponding

**TABLE 1: Selected Geometrical Parameters of the Free Hpz and $\sigma/\pi$ $[M(Hpz)]^+$ Complexes[a]**

| | | $[Cu(Hpz)]^+$ | | $[Ag(Hpz)]^+$ | |
|---|---|---|---|---|---|
| | Hpz | $\sigma$ | $\pi$ | $\sigma$ | $\pi$ |
| M−N(1) | | | 3.205 | | 3.412 |
| M−N(2) | | 1.856 | 3.271 | 2.129 | 3.256 |
| M−C(3) | | | 2.593 | | 2.548 |
| M−C(4) | | | 1.975 | | 2.279 |
| M−C(5) | | | 2.565 | | 2.972 |
| N(1)−N(2) | 1.356 | 1.366 | 1.369 | 1.363 | 1.358 |
| N(2)−C(3) | 1.340 | 1.353 | 1.322 | 1.351 | 1.335 |
| C(3)−C(4) | 1.415 | 1.398 | 1.459 | 1.400 | 1.454 |
| C(4)−C(5) | 1.386 | 1.389 | 1.435 | 1.387 | 1.414 |
| C(5)−N(1) | 1.361 | 1.350 | 1.335 | 1.352 | 1.342 |
| N(1)N(2)C(3) | 103.8 | 106.0 | 104.7 | 105.6 | 104.3 |
| N(2)C(3)C(4) | 112.0 | 110.0 | 111.9 | 110.4 | 111.4 |
| C(3)C(4)C(5) | 104.6 | 105.7 | 102.8 | 105.4 | 103.5 |
| C(4)C(5)N(1) | 106.0 | 107.5 | 106.0 | 107.3 | 106.0 |
| C(5)N(1)N(2) | 113.4 | 110.9 | 114.6 | 111.3 | 114.8 |

[a] Bond lengths and bond angles in Å and deg, respectively.

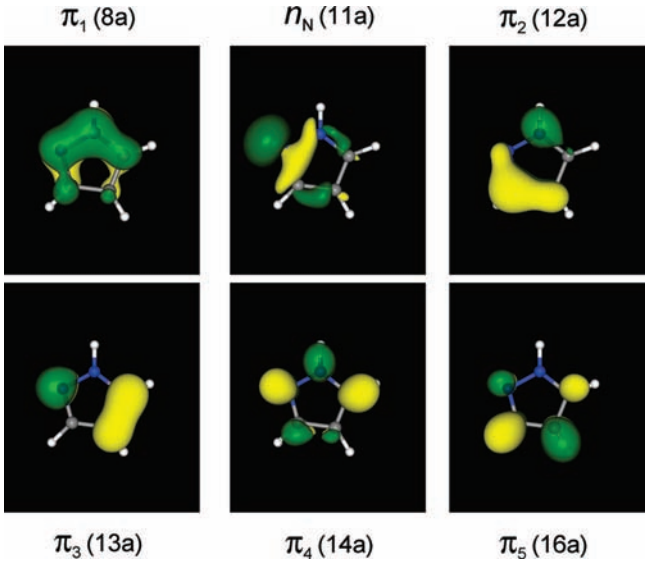


**Figure 2.** 3D contour plots of the Hpz $\pi_1-\pi_5$ MO's. The 3D plot of the $n_N$ is also included. Yellow (green) surfaces correspond to a constant positive (negative) value of 0.06 $e^{1/2}/Å^{3/2}$.

optimized coordinates are reported in Tables S2−S5), and selected geometrical parameters, Mulliken/Hirshfeld gross atomic charges and ETS contributions to the metal-ligand BE's are collected in Tables 1, 2 and 3, respectively. Structural perturbations undergone by the $C_3N_2$ pyrazole ring are rather similar for the two coordinative modes, except for the significant rehybridization of C(4) in $\pi$-$[M(Hpz)]^+$ (see Figure 3).[29] The analysis of COOP curves in Figure 4, and of gross atomic charge variations at C(4) on passing from the free ligand to the coordinated one (see Table 2) testifies that the C(4) rehybridization in $\pi$-$[M(Hpz)]^+$ has to be ultimately traced back to the concomitant Hpz $\pi_3 \rightarrow$ M(I) sp donation and M(I) d $\rightarrow \pi_5$ back-donation, with the former much stronger than the latter.[30] According to that, a lengthening of the C(4)−C(5) and C(3)−C(4) bond distances is computed on passing from the free to the coordinated Hpz.

A further point to be emphasized concerns the relevance of $\pi$ contributions to the metal-ligand bond in $\sigma$-$[M(Hpz)]^+$ complexes. More specifically, the inspection of Figure 5 testifies that, besides the $n_M \rightarrow {}^N$(sp) donation, high lying Hpz $\pi$ orbitals strongly localized on N(•) ($\pi_3$ and $\pi_4$ MO's, see Figure 2) significantly participate to the metal-ligand interaction.

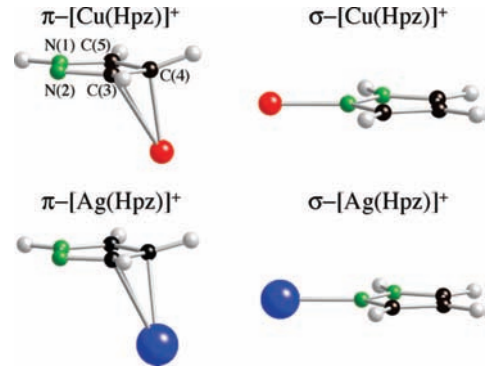


**Figure 3.** Schematic representations of the optimized structure of $\sigma/\pi$-$[M(Hpz)]^+$ complexes.

As far as BE values are concerned, the examination of data reported in Table 3 is particularly intriguing. In fact, despite BE's of $\sigma$ complexes being larger than those corresponding to the $\pi$ ones and $[Cu(Hpz)]^+$ BE's being larger than the $[Ag(Hpz)]^+$ ones, $\Delta E_{int}$ contributions show an opposite trend, thus indicating that each BE value is the result of a subtle balance of different contributions, with $\Delta E_{st}$ playing a very important role.

**3.2. tpm Conformational Flexibility.** The tpm X-ray crystal structure is characterized by a single pyrazolyl group with N(•) ($N_2^a$ in Figure 1b) in trans with respect to the hydrogen of the C−H fragment. This conformer has been labeled tpm-1,[31] and those corresponding to the $\kappa^2$-chelating (Figure 1c) and $\kappa^3$-tripodal (Figure 1d) coordinative modes have been tagged as tpm-2 and tpm-3, respectively. The tpm-0 conformer (see Figure 1a) is obviously the one with the three N(•) in cis with respect the methine fragment. Relative BE′s corresponding to tpm-0, tpm-1, and tpm-2 GS′s as well as to relevant saddle points are displayed in Figure 6 where sketches of the corresponding optimized molecular structures are also reported.[31,33] The tpm-3 conformer is not reported because it was found to be unstable.

Before going on, it deserves to be mentioned that the tpm-0 optimized structure is characterized by the presence of a $C_3$ axis with pyrazolyl fragments adopting a propeller-like orientation.[34] Such a result allowed us to label the linear combinations of Hpz-based frontier orbitals according to the a + e irreducible representations of the $C_3$ point group (see Figure 7). Interestingly, even though BE(tpm-0) and BE(tpm-1) are very close ($\Delta BE_{0,1}$ = BE(tpm-0) − BE(tpm-1) = 0.88 kcal/mol), tpm-1 corresponds to the absolute minimum not only in the solid state but also in the isolated molecule, thus confirming early semiempirical MNDO results of Claramunt et al.[36,37] This rather small difference is the balance of opposite effects involving $\Delta E_{st}$ (positive) and $\Delta E_{int}$ (negative) contributions in eq 1: $\Delta E_{st}$(tpm-0) is actually smaller than $\Delta E_{st}$(tpm-1) by 18.88 kcal/mol, and $\Delta E_{int}$(tpm-0) exceeds $\Delta E_{int}$(tpm-1) by 19.76 kcal/mol. Furthermore, consistently with the free rotation around $H_CC-N$ bonds proved by NMR measurements at room temperature,[38] the energy barrier associated to the tpm-0 → tpm-1 saddle point (TS1) is predicted very low (less than 2.5 kcal/mol).[40] We remark that, with the obvious exception of the LT parameter, all tpm internal coordinates are substantially unaffected by the tpm-0 → tpm-1 conversion (see Figure 8).

For the tpm-1 → tpm-2 conversion, two parameters can be chosen for the TS search, i.e., the rotations around either the $H_CC-N_1^b$ bond (TS2b) or the $H_CC-N_1^c$ one (TS2c, see Figure 1). The inspection of Figures 6 and 8 testifies that (i) TS2b and TS2c BE's are very similar and close to the TS1 one; (ii) $\Delta BE_{2,1} > \Delta BE_{0,1}$; and (iii) similarly to the tpm-0 → tpm-1 conversion,

**TABLE 2: Mulliken ($Q^M$) and Hirshfeld ($Q^H$) Charges of Selected Atoms of the Free Hpz and $\sigma/\pi$ $[M(Hpz)]^+$ Complexes**

| | Hpz | $[Cu(Hpz)]^+$ | | $[Ag(Hpz)]^+$ | |
|---|---|---|---|---|---|
| | | $\sigma$ | $\pi$ | $\sigma$ | $\pi$ |
| $Q^M_M$ ($Q^H_M$) | | 0.79 (0.54) | 0.51 (0.53) | 0.83 (0.60) | 0.63 (0.60) |
| $Q^M_{N(1)}$ ($Q^H_{N(1)}$) | 0.14 (−0.02) | 0.18 (0.02) | 0.17 (0.04) | 0.17 (0.01) | 0.17 (0.03) |
| $Q^M_{N(2)}$ ($Q^H_{N(2)}$) | −0.28 (−0.15) | −0.45 (−0.07) | −0.20 (−0.07) | −0.42 (−0.08) | −0.20 (−0.09) |
| $Q^M_{C(3)}$ ($Q^H_{C(3)}$) | 0.28 (−0.03) | 0.36 (0.03) | 0.43 (0.03) | 0.34 (0.02) | 0.33 (0.01) |
| $Q^M_{C(4)}$ ($Q^H_{C(4)}$) | 0.10 (−0.09) | 0.18 (−0.03) | −0.08 (−0.07) | 0.17 (−0.04) | −0.02 (−0.06) |
| $Q^M_{C(5)}$ ($Q^H_{C(5)}$) | 0.25 (−0.02) | 0.33 (0.05) | 0.41 (0.05) | 0.32 (0.04) | 0.37 (0.04) |

**TABLE 3: Binding Energy Contributions in kcal/mol for $\sigma/\pi$ $[M(Hpz)]^+$ Complexes**

| | $[Cu(Hpz)]^+$ | | $[Ag(Hpz)]^+$ | |
|---|---|---|---|---|
| | $\sigma$ | $\pi$ | $\sigma$ | $\pi$ |
| $\Delta E_{st}$ | −15.3 | −1.2 | 26.1 | 43.2 |
| $\Delta E_{int}$ | −59.5 | −65.1 | −79.4 | −88.2 |
| $\Delta E_{prep}$ | 1.1 | 5.9 | 0.8 | 3.2 |
| BSSE | 1.2 | 1.7 | 0.3 | 0.4 |
| BE | −72.5 | −58.7 | −52.2 | −41.3 |

the tpm-1 → tpm-2 one negligibly affects tpm internal coordinates (see Figure 8).

The $\Delta E_{int}$(tpm-1) and $\Delta E_{int}$(tpm-2) contributions are very similar (the latter is 0.25 kcal/mol larger than the former), whereas $\Delta E_{st}$(tpm-2) exceeds $\Delta E_{st}$(tpm-1) by 2.75 kcal/mol. Such a result ultimately indicates that the lower stability of tpm-2 compared to tpm-1 has to be traced back to the repulsive

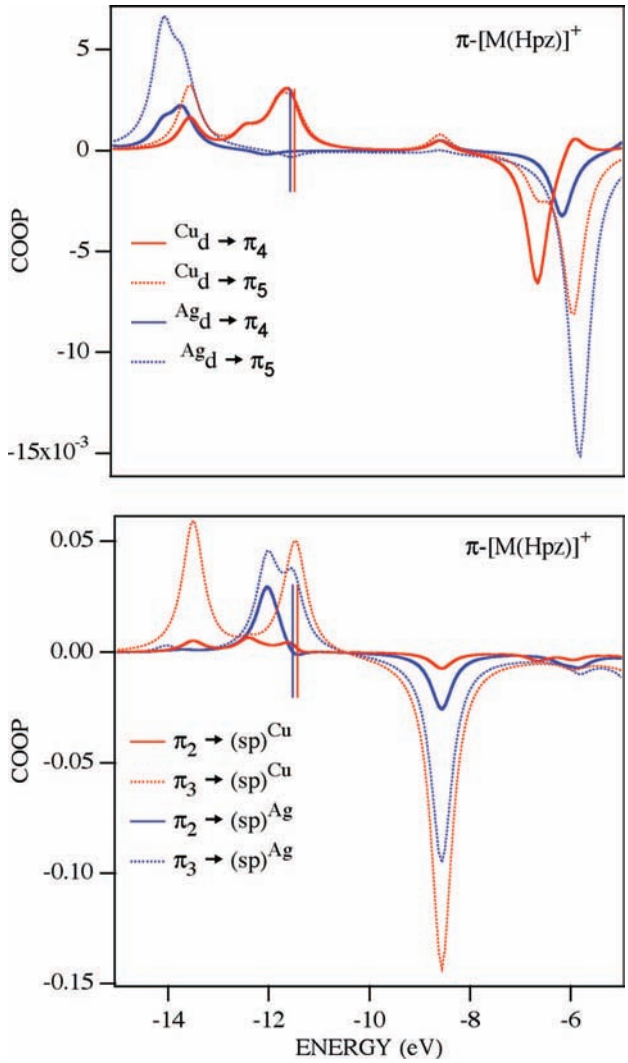


**Figure 4.** M(I) d → $\pi^*$ Hpz (up) and Hpz $\pi$ → sp M(I) (down) COOP's in $\pi$-$[M(Hpz)]^+$ complexes. Bonding (antibonding) states correspond to positive (negative) peaks. Vertical bars represent the HOMO energies.

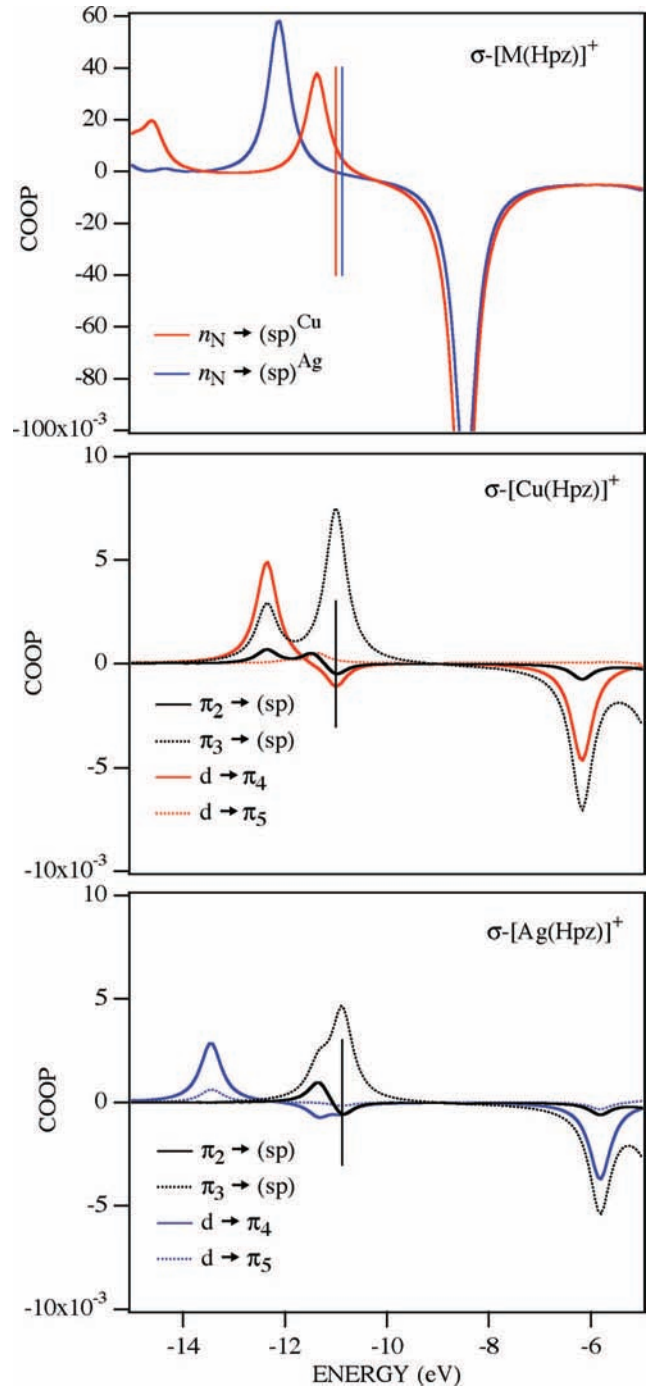


**Figure 5.** Hpz $n_N$ → sp M(I) (up) and [Hpz $\pi$ → sp M(I)]/[M(I) d → $\pi^*$ Hpz] (middle and down) COOP's in $\sigma$-$[M(Hpz)]^+$ complexes.

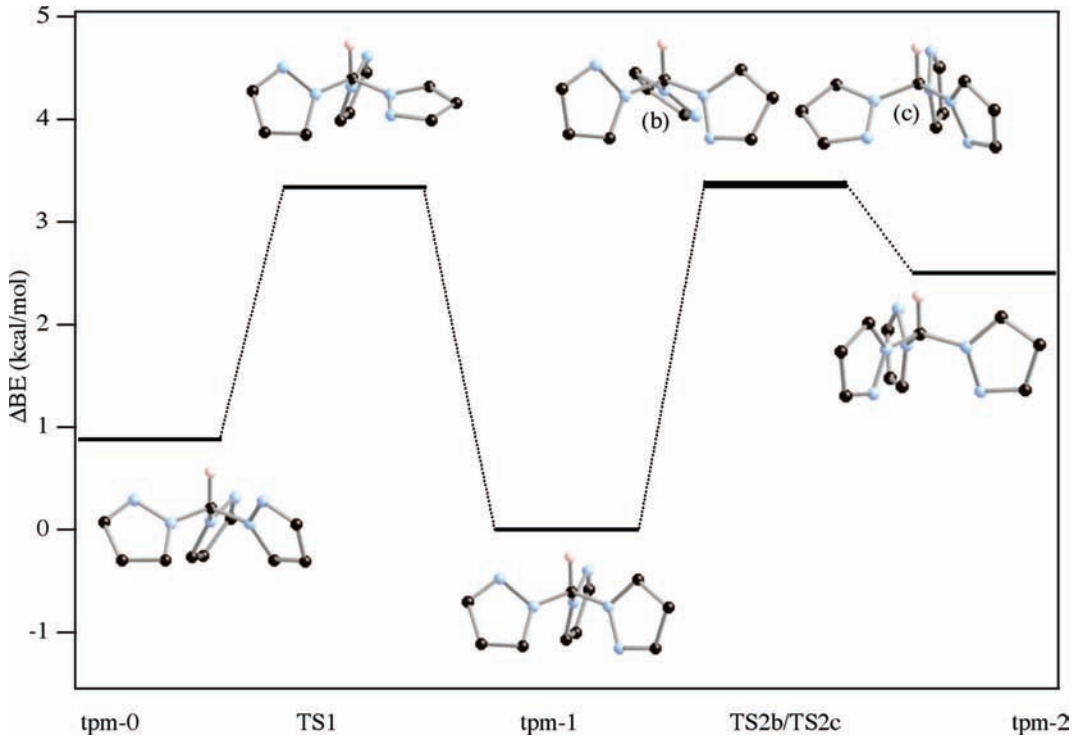


**Figure 6.** Relative BE values of tpm-0, TS1, tpm-1, TS2b/TS2c, tpm-2. The zero energy value corresponds to the tpm-1 BE. Schematic representations of the corresponding optimized structure are also displayed.

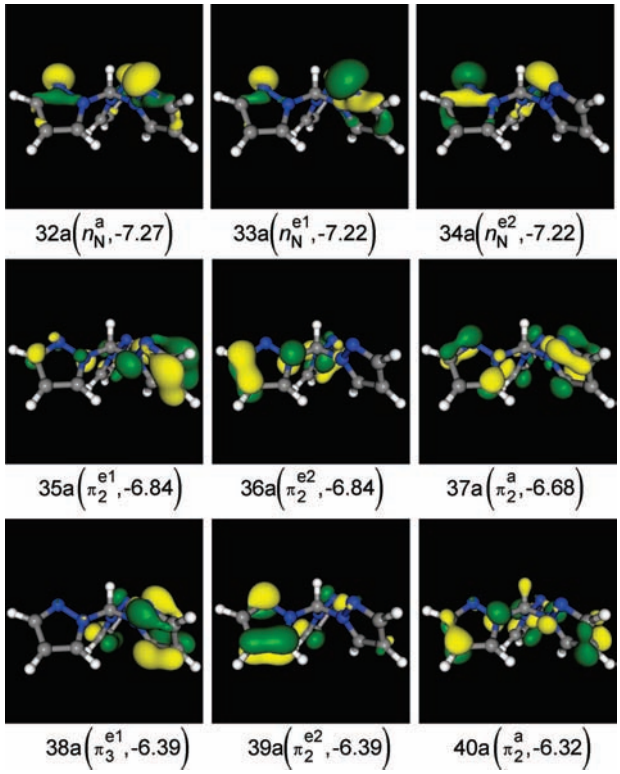


**Figure 7.** 3D contour plots of tpm-0 outermost occupied MO's. In parentheses is reported the energy in electronvolt of each level and its parenthood with the Hpz-based orbitals. Contour plot parameters are the same of Figure 2.

interaction between the two N(•) $n_N$ in trans to the $H_CC$ fragment ($\Delta E_{Pauli}$(tpm-1) and $\Delta E_{Pauli}$(tpm-2) differ by 3.18 kcal/mol).

As a whole, the above described theoretical results outline that, though common, the tpm $\kappa^3$-tripodal coordinative mode is unlikely to be achieved through the direct interaction of M(I) with tpm having a tpm-3 arrangement.

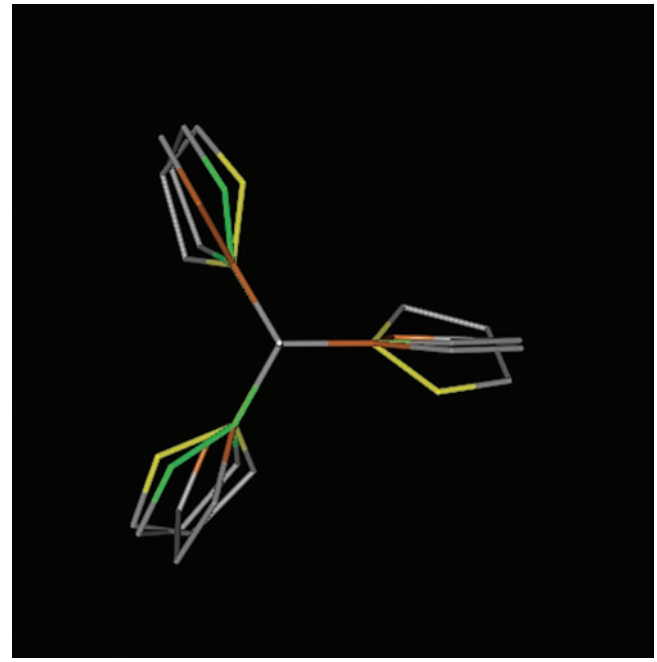

**Figure 8.** Superimposed licorice representation of tpm-0 (N atoms in yellow), tpm-1 (N atoms in light green), and tpm-2 (N atoms in orange) optimized structures. The view is along the C−$H_C$ bond. Hydrogen atoms of pyrazolyl fragments are not displayed for the sake of clarity.

**3.3. [Cu(tpm)]$^+$ and [Ag(tpm)]$^+$ Complexes.** Reger and coworkers first reported the synthesis and characterization of cationic [tris(pyrazol-1-yl)methane]M(I) (M = Cu,[41a] Ag[41b]) complexes about ten years ago, and although a lot of chemistry has been published on this subject since then,[42] not only are theoretical investigations devoted to tpm metal complexes very few in number,[6e,32,43] but none of them has been specifically dedicated to the analysis of the metal−ligand bonding scheme.

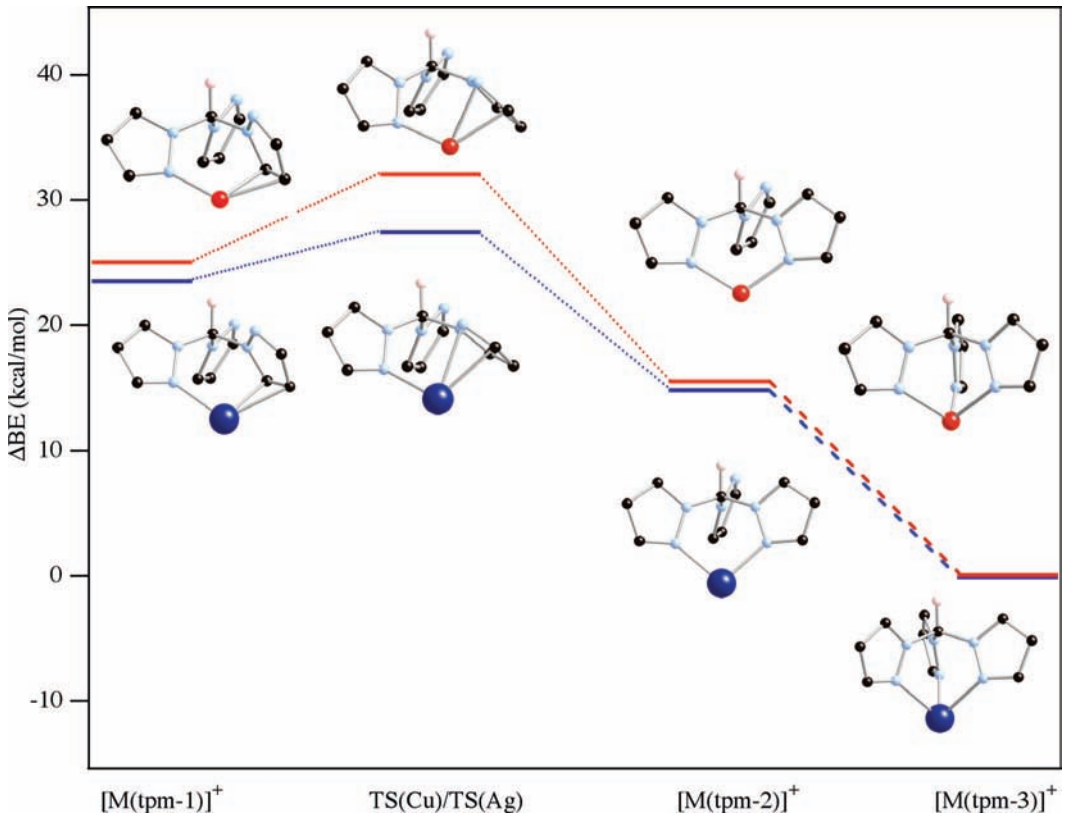


**Figure 9.** Relative BE values of $[M(tpm\text{-}1)]^+$, TS(M), $[M(tpm\text{-}2)]^+$, and $[M(tpm\text{-}3)]^+$. The zero energy value corresponds to the $[M(tpm\text{-}3)]^+$ BE. Schematic representations of the corresponding optimized structure are also displayed. Red and blue spheres correspond to copper and Silver atoms, respectively.

**TABLE 4: Binding Energy Contributions in kcal/mol for $[M(tpm)]^+$ Complexes**

| | $[M(tpm\text{-}1)]^+$ | TS(M) | $M(tpm\text{-}2)]^+$ | $M(tpm\text{-}3)]^+$ |
|---|---|---|---|---|
| $^{Cu}\Delta E_{st}$ | −0.87 | −4.97 | −14.13 | −30.14 |
| $^{Cu}\Delta E_{int}$ | −97.18 | −86.05 | −93.47 | −92.95 |
| $^{Cu}\Delta E_{prep}$ | 6.92 | | 4.67 | |
| $^{Cu}$BSSE | 2.79 | | 2.46 | |
| $^{Cu}$BE | −88.34 | | −100.47 | |
| $^{Ag}\Delta E_{st}$ | 64.76 | 51.51 | 50.27 | 43.92 |
| $^{Ag}\Delta E_{int}$ | −132.66 | −115.46 | −126.87 | −135.32 |
| $^{Ag}\Delta E_{prep}$ | 4.50 | | 3.91 | |
| $^{Ag}$BSSE | 0.66 | | 0.52 | |
| $^{Ag}$BE | −62.74 | | −72.17 | |

The strength and the nature of the M(I)−tpm bond in $[M(tpm\text{-}n)]^+$ ($n$ = 1, 2, and 3) have been obtained through the ETS scheme by considering M(I) and tpm as interacting fragments.[12] Optimized coordinates of $[M(tpm\text{-}n)]^+$ species and of TS(Cu) and TS(Ag) saddle points corresponding to the $[M(tpm\text{-}1)]^+ \rightarrow [M(tpm\text{-}2)]^+$ conversions are collected in Tables S12−S19. Relative BE's are displayed in Figure 9 where sketches of the corresponding optimized molecular structures are also displayed.

The comparison between data of Figure 9 and Figure 6 reveals that, as a consequence of the M(I)−tpm interaction, the $[M(tpm\text{-}2)]^+$ molecular ion is more stable than the $[M(tpm\text{-}1)]^+$ one, reversing the energy order found for the free ligand. Quite unexpectedly, this is not due to covalent but to steric effects (see Table 4). In this regard, theoretical results pertaining to $[M(tpm\text{-}n)]^+$ molecular ions substantially mirror those already discussed for the $\sigma/\pi$-$[M(Hpz)]^+$ species: despite the Ag(I)−ligand interaction being stronger than the Cu(I)−ligand one, $\Delta E_{st}$ contributions play a crucial role in determining final BE's values.

Interestingly, even though $[Cu(tpm\text{-}2)]^+$ and $[Ag(tpm\text{-}2)]^+$ correspond to local minima, we were unable to find the saddle point corresponding to the $[M(tpm\text{-}2)]^+ \rightarrow [M(tpm\text{-}3)]^+$ conversion because of the flatness of the potential energy surface in that region. This indicates that, when the $\kappa^2$-complex is formed, either from the interaction of M(I) with tpm-2 or through the $[M(tpm\text{-}1)]^+ \rightarrow [M(tpm\text{-}2)]^+$ conversion, the $\kappa^3$-tripodal species will be readily formed. However, the $[M(tpm\text{-}2)]^+ \rightarrow [M(tpm\text{-}3)]^+$ conversion could be hampered by several reasons such as (i) the coordinative saturation of the metal center by concurrent ligands; (ii) the coordination of the N(•) of the third pyrazolyl group to a different metal center; (iii) steric factors determined by bulky substituents of tpm.[44] In this regard, it has to be noted that, despite the M(I) coordinative unsaturation, the optimized geometrical parameters of $[Ag(tpm\text{-}2)]^+$, $[Cu(tpm\text{-}3)]^+$, and $[Ag(tpm\text{-}3)]^+$ agree satisfactorily with those experimentally determined for Ag(I) $\kappa^2$-[44i,l] and M(I) $\kappa^3$-complexes.[41,44i,l,45] No X-ray data pertaining to Cu(I) $\kappa^2$-complexes are available for comparison to our knowledge.

Further insights into to the M(I)-tpm bonding scheme can be gained by referring to Figures 10 and 11 where $[M(tpm\text{-}n)]^+$ PDOS and COOP curves are displayed. The inspection of the two figures[46] testifies to (i) the leading role played by the tpm → M(I) donation, mainly $\sigma$ in character, (ii) the stronger involvement of the M(I) s AO compared to the one of the M(I) p AO's, and (iii) the negligible contribution provided by the M(I) → tpm back-donation.

## 4. Concluding Remarks

In this contribution we have presented and discussed the results of a series of first-principle numerical experiments

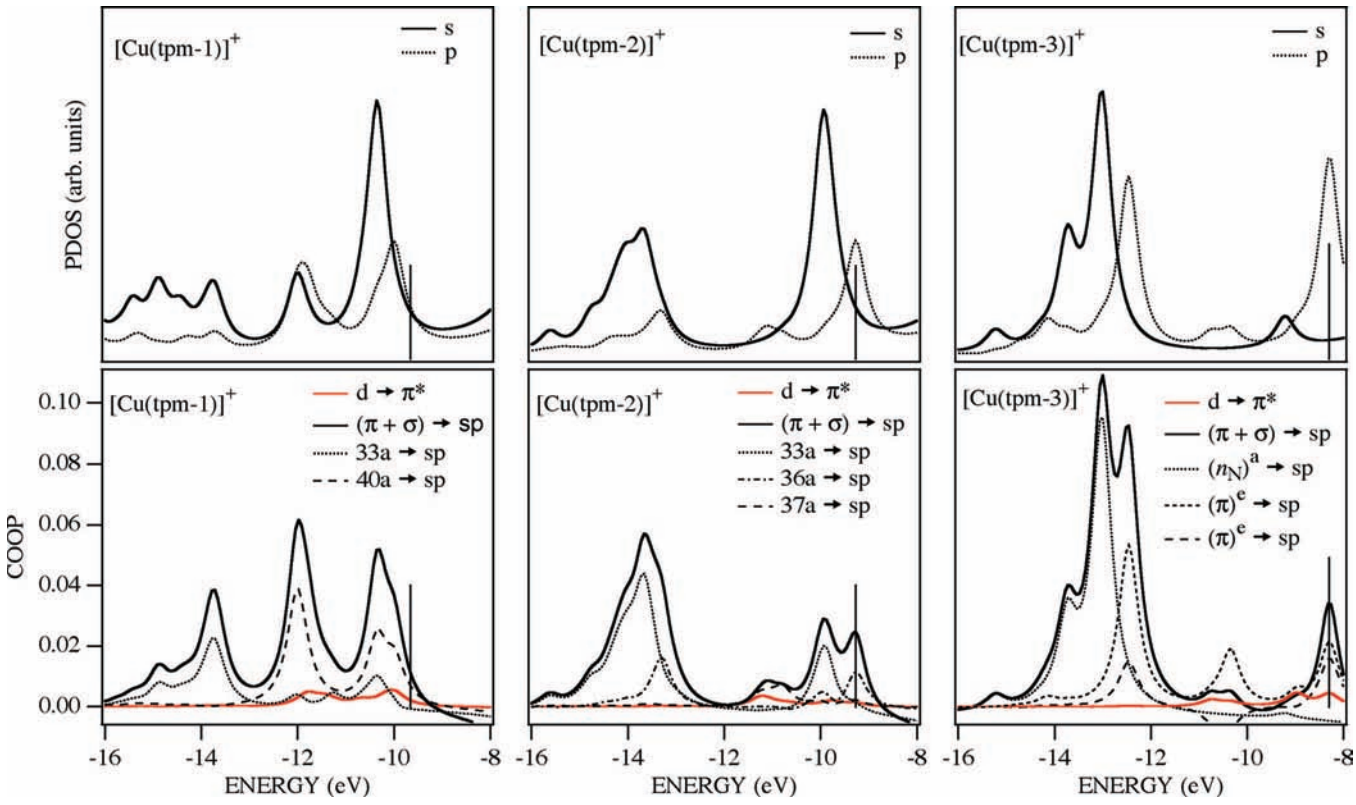


**Figure 10.** s and p PDOS (up) and major components of tpm $\sigma \rightarrow$ sp Cu(I), tpm $\pi \rightarrow$ sp Cu(I), and Cu(I) d $\rightarrow \pi^*$ tpm (down) for $[Cu(tpm\text{-}n)]^+$ ($n$ = 1, 2, and 3).

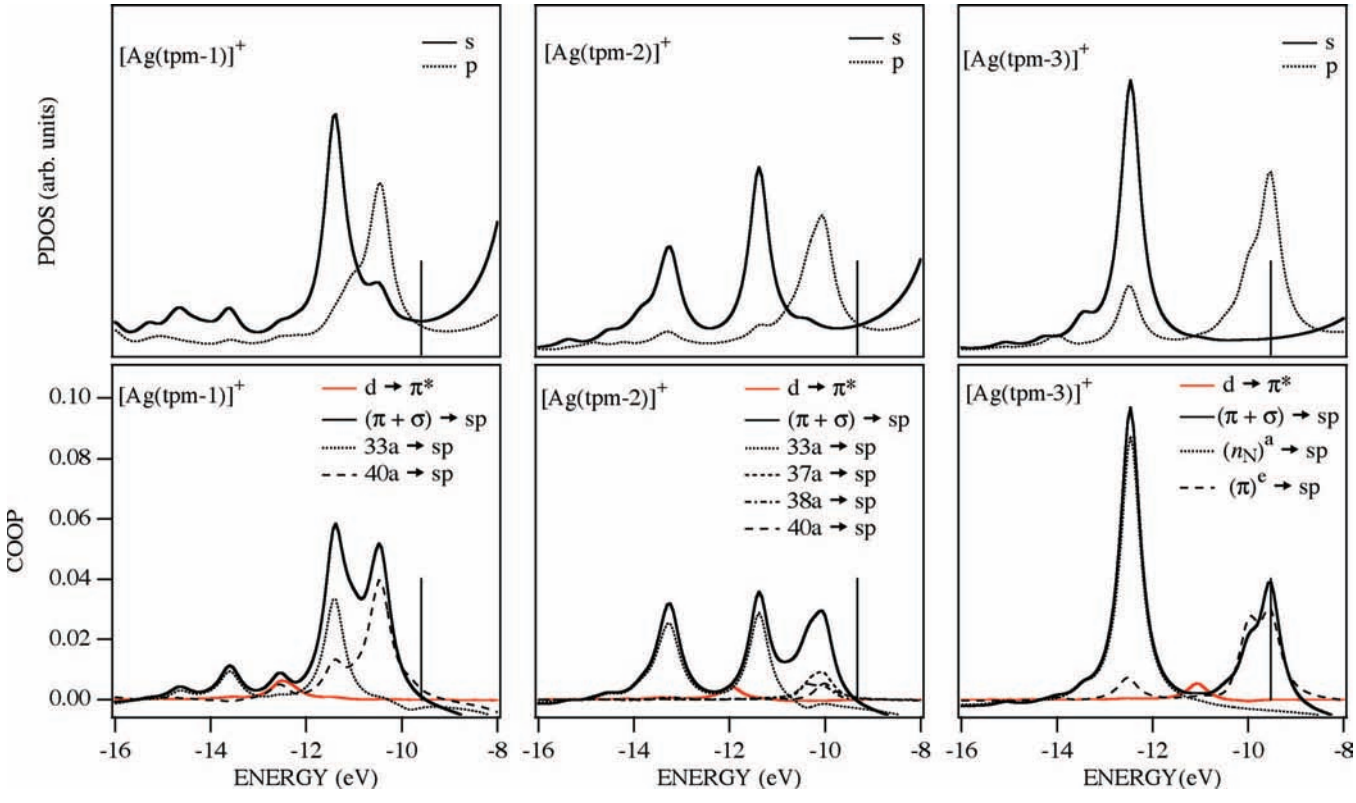


**Figure 11.** s and p PDOS (up) and major components of tpm $\sigma \rightarrow$ sp Ag(I), tpm $\pi \rightarrow$ sp Ag(I), and Ag(I) d $\rightarrow \pi^*$ tpm (down) for $[Ag(tpm\text{-}n)]^+$ ($n$ = 1, 2, and 3).

carried out on the free Hpz and tpm ligands, as well as on their Cu(I) and Ag(I) complexes. We gave detailed information about the energetics of interconversions among conformers, both for the free and for the coordinated ligands. Finally, we analyzed the M−ligand interaction showing that, independently of the coordinative mode, this is dominated by the ligand → M(I) $\sigma$ donation with negligible contribution from back-donation.

**Acknowledgment.** This work was partially supported by the Italian PRIN founding n. 2006038447. The "Laboratorio Interdipartimentale di Chimica Computazionale" (LICC) at the Department of Chemistry of the University of Padova is acknowledged for support of the computer facilities.

**Supporting Information Available:** Optimized coordinates of Hpz, $\pi$-[Cu(Hpz)]$^+$, $\sigma$-[Cu(Hpz)]$^+$, $\pi$-[Ag(Hpz)]$^+$, $\sigma$-[Ag(Hpz)]$^+$, tpm-0, tpm-1, tpm-2, TS1, TS2b, TS2c, [Cu(tpm-1)]$^+$, TS(Cu), [Cu(tpm-2)]$^+$, [Cu(tpm-3)]$^+$, [Ag(tpm-1)]$^+$, TS(Ag), [Ag(tpm-2)]$^+$, and [Ag(tpm-3)]$^+$ are reported in Tables S1−S19, respectively. The comparison between the Hpz VUV-absorption spectrum and TD-DFT results is displayed in Figure S1. This material is available free of charge via the Internet at http://pubs.acs.org.

## References and Notes

(1) (a) Pettinari, C.; Pettinari, R. *Coord. Chem. Rev.* **2005**, *249*, 525, and references therein reported. (b) Pettinari, C.; Santini, C. *Compr. Coord. Chem. II* **2004**, *1*, 159. (c) Trofimenko, S. *Scorpionates, The coordination Chemistry of Polypyrazolylborate Ligands*; Imperial College Press: London, 1999. (d) Pettinari, C. *Scorpionates II: Chelating borate ligands*; World Scientific Publishing: New York, 2008. (e) Trofimenko, S. J. *Chem. Educ.* **2005**, *82*, 1715. (f) Murtuza, S.; Casagrande, O. L., Jr.; Jordan, R. F. *Polym. Mater. Sci. Eng.* **2001**, *84*, 109. (g) Santos, I.; Paulo, A.; Correia, J. D. *Top. Curr. Chem.* **2005**, *252*, 45. (h) Kitano, T.; Wada, H.; Mukai, H.; Ueda, K.; Sohrin, Y. *Anal. Sci.* **2001**, *17*, i1113. (i) de la Lande, A.; Gérard, H.; Moliner, V.; Izzet, G.; Reinaud, O.; Parisel, O. J. *Biol. Inorg. Chem.* **2006**, *11*, 593.

(2) tp and tpm may also act as $\kappa^2$-ligands bonded to a single metal ($\kappa^2$-chelating), as $\kappa^1$-$\kappa^2$-ligands bridging two metals or, hardly ever, as $\kappa^1$-ligands depending on the steric congestion around the metal center and the number of donor substituents on the central atom X, which may be P and Ga other than B and C (see refs 1 and 3).

(3) (a) Paneque, M.; Sirol, S.; Trujillo, M.; Gutiérrez-Puebla, E.; Monge, M. A.; Carmona, E. *Angew. Chem. Int. Ed.* **2000**, *39*, 218. (b) Ellis, D. D.; Jeffery, J. C.; Jelliss, P. A.; Kautz, J. A.; Stone, F. G. A. *Inorg. Chem.* **2001**, *40*, 2041.

(4) McLauchlan, C. C.; Varda, A. N.; Giles, J. R. *Acta Crystallogr, Sect. E: Struct. Rep. Online* **2004**, *60*, o1419.

(5) The relative position of pyrazolyl fragments in substituted and unsubstituted tp and tpm is strongly influenced by the steric hindrance of substituents possibly present on the ring carbon atoms.[6]

(6) (a) Dias, H. V. R.; Jin, W.; Kim, H.-J.; Lu, H.-L. *Inorg. Chem.* **1996**, *35*, 2317. (b) Reger, D. L.; Semeniuc, R. F.; Smith, M. D. *Eur. J. Inorg. Chem.* **2003**, 3480. (c) Declercq, J. P.; van Meerssche, M. *Acta Crystallogr., Sect. C: Cryst. Struct. Commun.* **1984**, *40*, 1098. (d) Ochando, L. E.; Rius, J.; Louer, D.; Claramunt, R. M.; Lopez, C.; Elguero, J.; Amigo, J. M. *Acta Crystallogr., Sect. B: Struct. Sci.* **1997**, *53*, 939. (e) Fujisawa, K.; Ono, T.; Ishikawa, Y.; Amir, N.; Miyashita, Y.; Okamoto, K.; Lehnert, N. *Inorg. Chem.* **2006**, *45*, 1698. (f) Hammes, B. S.; Luo, X.; Carrano, M. W.; Carrano, C. J. *Angew. Chem. Int. Ed.* **2002**, *41*, 3259.

(7) De Bari, H.; Zimmer, M. *Inorg. Chem.* **2004**, *43*, 3344 Database searches and analyses carried out by the authors were done by using the Conquest and Vista programs associated with Cambridge Structural Database13 (CSD) v5.24.

(8) Here the negatively charged tp ligand is not taken into account to avoid the use of extended basis sets.

(9) We are perfectly aware that Hpz electronic properties have been the subject of several theoretical[10] and experimental[11] investigations, but we decided to extend our study to this molecule to compare homogeneous theoretical data.

(10) (a) Kuznetsov, M. L.; Dementiev, A. I.; Krasnoshchoikov, S. V. *J. Mol. Struct. (THEOCHEM)* **1998**, *453*, 17. (b) da Silva, G.; Moore, E. E.; Bozzelli, J. W. *J. Phys. Chem. A* **2006**, *110*, 13979. (c) El-Azhary, A. A. *Spectrochim. Acta A* **2003**, *59*, 2009.

(11) Walker, I. C.; Palmer, M. H.; Hubin-Franskin, M. -J.; Delwiche, J. *Chem. Phys. Lett.* **2003**, *367*, 517.

(12) Amsterdam Density Functional (ADF) version 2007.01. http://www.scm.com.

(13) (a) van Lenthe, E.; Baerends, E. J.; Snijders, J. G. *J. Chem. Phys.* **1993**, *99*, 4597. (b) van Lenthe, E.; Baerends, E. J.; Snijders, J. G. *J. Chem. Phys.* **1994**, *101*, 9783. (c) van Lenthe, E.; Ehlers, A. W.; Baerends, E. J.; Snijders, J. G. *J. Chem. Phys.* **1999**, *110*, 8543.

(14) (a) Becke, A. D. *Phys Rev A* **1988**, *38*, 3098. (b) Perdew, J. P. *Phys. Rev. B* **1986**, *33*, 8822.

(15) A LT calculation implies a linear change of a selected LT parameter from its initial to its final value through a specified number of equidistant steps.

(16) van Lenthe, E.; Baerends, E. J. *J. Comput. Chem.* **2003**, *24*, 1142.

(17) Ziegler, T.; Rauk, A. *Theor. Chim. Acta* **1977**, *46*, 1.

(18) Rosa, A.; Ehlers, A. W.; Baerends, E. J.; Snijders, J. G.; te Velde, G. *J. Phys. Chem.* **1996**, *100*, 5690.

(19) Mulliken, R. S. *J. Chem. Phys.* **1955**, *23*, 1833.

(20) Hoffmann, R. *Solids and Surfaces: A Chemist's View of Bonding in Extended Structures*; VCH: New York, 1988.

(21) Pauling electronegativity for most of the elements are reported in the following website http://www.webelements.com/.

(22) Hirshfeld, F. L. *Theor. Chim. Acta* **1977**, *44*, 129.

(23) Da Silva, G.; Moore, E. E.; Bozzelli, J. W. *J. Phys. Chem. A* **2006**, *110*, 13979.

(24) IE's have been evaluated by using the Slater transition state procedure,[25] and lowest lying excitation energies and corresponding oscillator strengths were evaluated by employing the time dependent DFT (TD-DFT) approach.[26]

(25) Slater, J. C. *Quantum Theory of Molecules and Solids. The Self-Consistent Field For Molecules and Solids*; McGraw-Hill: New York, 1974, Vol. 4.

(26) Gross, E. K. U.; Dobson, J. F.; Petersilka, M. In *Density Functional Theory*; Nalewajski, R. F., Ed.; Springer, Heidelberg, 1996.

(27) The theoretical (experimental)[28] $\mu_{Hpz}$ value is 2.282 (2.214 ± 0.015) D, theoretical (experimental)[11] IEs of $n_N$, $\pi_2$, and $\pi_3$ frontier MO′s are 10.68 (10.65), 9.74 (9.88), and 9.48 (9.15) eV, respectively. The comparison between theoretical and experimental[11] absorption spectrum in the 5−9 eV energy range is reported as Supporting Information.

(28) Kirchhoff, W. H. *J. Am. Chem. Soc.* **1967**, *89*, 1312.

(29) In the [Cu(Hpz)]$^+$ ([Ag(Hpz)]$^+$) $\pi$-complex the N(1)N(2)C(3)C(4) and N(2)N(1)C(5)C(4) dihedral angles are 1.5° (1.3°) and 0.1° (0.0°), respectively, and the N(2)C(3)C(4)$H_{C(4)}$ and N(1)C(5)C(4)$H_{C(4)}$ ones are 152.5° and 152.6° (both 160.9°), respectively. Moreover, the CuC(4)$H_{C(4)}$ (AgC(4)$H_{C(4)}$) bond angle corresponds to 102.4° (99.7°).

(30) Both $\pi_3$ and $\pi_5$ MO′s are strongly localized on the C(4) atom (see Figure 2).

(31) The tpm-1 conformer has not been associated to the $\kappa^1$-mode because, to our knowledge, the only structurally ascertained compound with a scorpionate ligand truly $\kappa^1$-monodentate is the Rh(I) complex reported by Paneque et al.,[3a] where the metal ion and the H atom of the B−H fragment of the hydrotris(3,5-dimethylpyrazolyl)borato are in a cis arrangement. Even if Reger et al.[32] recently revealed an unprecedented coordination mode of a tpm analogue in $\{[Ph_2(O)POCH_2C(pz)_3Ag]_2(THF)_2\}(BF_4)_2$.

(32) Reger, D. L.; Semeniuc, R. F.; Captain, B.; Smith, M. D. *Inorg. Chem.* **2005**, *44*, 2995.

(33) Optimized coordinates of tpm-0, tpm-1, tpm-2, TS1, and TS2 are reported in Tables S6−S11.

(34) The propeller-like configuration is the same obtained, through molecular mechanics calculations, for the global minimum of free tp by Sohrin et al.[35]

(35) Sohrin, Y.; Kokusen, H.; Matsd, M. *Inorg. Chem.* **1995**, *34*, 3928.

(36) Claramunt, R. M.; Elguero, J.; Fabre, M. J.; Foces-Foces, C.; Cano, F. H.; Fuentes, I. H.; Jaime, C.; López, C. *Tetrahedron* **1989**, *45*, 7805.

(37) Even though MNDO calculations of Claramunt et al.[36] succeeded in foreseen a tpm-1-like arrangement as the most stable conformation of the free ligand, they computed a $\Delta BE_{0,1}$ (2.62 kcal/mol) value significantly higher than that herein reported (0.88 kcal/mol).

(38) The $^1$H NMR spectrum of tpm at room temperature shows a singlet for the CH methyne proton and two pseudodoublet and one pseudotriplet for the heterocyclic ring protons.[39ab] The three pyrazolyl fragments are all equivalent likely as a consequence of the rapid rotation around the H−C axis. In this regard, Reger suggested that within each tpm unit, the orientation of the three pyrazolyl moieties has a propeller arrangement.[39c]

(39) (a) Elguero, J.; Claramunt, R. M.; Garcerán, R.; Julià, S.; Avila, L.; del Mazo, J. M. *Magn. Reson. Chem.* **1987**, *25*, 260. (b) Otting, G.; Messerle, B. A.; Soler, L. P. *J. Am. Chem. Soc.* **1996**, *118*, 5096. (c) Reger, D. L.; Grattan, T. C. *Synthesis* **2003**, *3*, 350.

(40) The tpm-0 → tpm-1 conversion has been evaluated by starting from tpm-0 and specifying, as single LT parameter, the rotation angle around a $H_CC-N$ bond.

(41) (a) Reger, D. L.; Collins, J. E.; Rheingold, A. L.; Liable-Sands, L. M. *Organometallics* **1996**, *15*, 2029. (b) Reger, D. L.; Collins, J. E.; Rheingold, A. L.; Liable-Sands, L. M.; Yap, G. P. A. *Organometallcs* **1997**, *16*, 349.

(42) (a) Reger, D. L.; Watson, R. P.; Smith, M. D. *Inorg. Chem.* **2006**, *45*, 10077, and references therein reported. (b) Reger, D. L.; Semeniuc, R. F.; Gardinier, J. R.; O'Neal, J.; Reinecke, B.; Smith, M. D. *Inorg. Chem.* **2006**, *45*, 4337, and references therein reported.

(43) (a) Chu, H. S.; Xu, Z.; Ng, S. M.; Lau, C. P.; Lin, Z. *Eur. J. Inorg. Chem.* **2000**, 993. (b) Lehnert, N.; Cornelissen, U.; Neese, F.; Ono, T.; Noguchi, Y.; Okamoto, K.; Fujisawa, K. *Inorg. Chem.* **2007**, *46*, 3916.

(44) (a) Canty, A. J.; Minchin, N. J.; Patrick, J. M.; Healy, P. C.; White, A. H. *J. Chem. Soc., Dalton Trans.* **1982**, 1795. (b) Canty, A. J.; Minchin, N. J.; Patrick, J. M.; White, A. H. *J. Chem. Soc., Dalton Trans.* **1983**, 1253. (c) Canty, A. J.; Minchin, N. J.; Engelhardt, L. M.; Skelton, B. W. *J. Chem. Soc., Dalton Trans.* **1986**, 645. (d) Adams, C. J.; Connelly, N. G.; Emslie, D. J. H.; Hayward, O. D.; Manson, T.; Orpen, A. G.; Rieger, P. H. *Dalton Trans.* **2003**, 2835. (e) Bhambri, S.; Tocher, D. A. *J. Chem. Soc., Dalton Trans.* **1997**, 3367. (f) Iengo, E.; Zangrando, E.; Baiutti, E.; Munini, F.; Alessio, E. *Eur. J. Inorg. Chem.* **2005**, 1019. (g) Bellachioma, G.; Cardaci, G.; Gramlich, V.; Ruegger, H.; Terenzi, S.; Venanzi, L. M. *Organometallics* **1997**, *16*, 2139. (h) Titze, C.; Hermann, J.; Vahrenkamp, H. *Chem. Ber.* **1995**, *128*, 1095. (i) Reger, D. L.; Semeniuc, R. F.; Smith, M. D. *Eur. J. Inorg. Chem.* **2003**, 3480. (j) Reger, D. L.; Semeniuc, R. F.; Captain, B.; Smith, M. D. *Inorg. Chem.* **2005**, *44*, 2995. (k) Reger, D. L.; Semeniuc, R. F.; Little, C. A.; Smith, M. D. *Inorg. Chem.* **2006**, *45*, 7758. (l) Cingolani, A.; Effendy; Martini, D.; Pellei, M.; Pettinari, C.; Skelton, B. W.; White, A. H. *Inorg. Chim. Acta* **2002**, *328*, 87.

(45) (a) Cvetkovic, M.; Batten, S. R.; Moubaraki, B.; Murray, K. S.; Spiccia, L. *Inorg. Chim. Acta* **2001**, *324*, 131. (b) Reger, D. L.; Semeniuc, R. F.; Smith, M. D. *Rev. Roum. Chim.* **2002**, *47*, 1037. (c) Choi, I. Y.; Ahn, S.; Seo, J.; Park, K.-M. *Bull. Korean Chem. Soc.* **2004**, *25*, 1065. (d) Fujisawa, K.; Ono, T.; Ishikawa, Y.; Amir, N.; Miyashita, Y.; Okamoto, K.; Lehnert, N. *Inorg. Chem.* **2006**, *45*, 1698. (e) Kaim, W.; Titze, C.; Schurr, T.; Sieger, M.; Lawson, M.; Jordanov, J.; Rojas, D.; Garcia, A. M.; Manzur, J. Z. *Anorg. Allg. Chem.* **2005**, *631*, 2568.

(46) The absence of any local symmetry in $[M(tpm\text{-}1)]^+$ and $[M(tpm\text{-}2)]^+$ allows a quite extensive mixing among highest occupied tpm based MO′s ($n_N$ and $\pi_2/\pi_3$ linear combinations). MO′s have been then labeled in Figures 10 and 11 by simply referring to their energy order in the free tpm fragment.

JP801902C